Lipase-Driven Deconstruction of Polyether Polyurethane Foams through Alcoholysis toward a Closed-Loop Recycling

Riccardo Moro[a], Daniel Grajales-Hernández[a], Katarzyna Świderek[b], Ion Olazabal[c], Gabriel Perli[c], Andrea Rizzo[a], Mariana Armendáriz-Ruiz[a], Rut Fernández-Marín[a], Javier Calvo[a], Vicent Moliner[b]*, Haritz Sardón[c]*, Fernando López-Gallego[a,d]*

[a] Center for Cooperative Research in Biomaterials (CIC biomaGUNE), Basque Research and Technology Alliance (BRTA), Paseo de Miramon 182, 20014, Donostia, Spain
[b] BioComp Group, Institute of Advanced Materials (INAM), Universitat Jaume I, 12071 Castellón, Spain.
[c] *POLYMAT and Department of Polymers and Advanced Materials: Physics, Chemistry and Technology, Faculty of Chemistry, University of the Basque Country UPV/EHU, Paseo Manuel de Lardizábal, 3, 20018 Donostia-San Sebastián, Spain.*
[d] Ikerbasque, Basque Foundation for Science, 48011 Bilbao, Spain

ABSTRACT

Polyether polyurethane foams are widely used materials in everyday life, yet they are highly recalcitrant and difficult to recycle. Until now, no efficient bioprocess currently exists for their depolymerization. Lastly, the use of enzymes has revolutionized plastic recycling, but their application to polyurethanes remains in its infancy. In this work, we selected some enzymes capable of cleaving urethane bonds through alcoholysis, a mechanism that goes beyond conventional enzymatic hydrolysis. Among them, two lipases from *Thermomyces lanuginosus* and *Rhizopus oryzae* proved particularly promising when using methanol and ethanol as reaction agents. These enzymes successfully degraded polyether polyurethane foams, releasing polyols and alkyl carbamates. The recovered polyols could be isolated and subsequently reused in a new polymerization process, generating partially recycled foams. This enzymatic solvolysis approach in alcohol media was extended to non-isocyanate polyurethane foams, opening new paths for depolymerizing and recycling complex plastics, thereby contributing to a more circular plastic economy.

INTRODUCTION

Over the past 70 years, synthetic polymer production has grown exponentially, making plastics fundamental to the modern economy.(*1*) However, most plastics are produced, used once, and discarded, following a linear, fossil-based model that has led to a global waste crisis. Particularly, polyurethanes (PURs) are widely used for their durability and versatility in products such as foams (e.g., mattresses, insulation), thermoplastics (e.g., sports shoes), and coatings (e.g., paints, adhesives).(*2*) Despite their utility, PURs are mainly synthesized via polycondensation of fossil-derived diisocyanates and polyols,(*3*) with diisocyanates posing major environmental and safety risks due to their toxicity and hazardous production processes.(*4-8*)

To overcome the sustainability and safety issues underlying PUR, non-isocyanate polyurethanes (NI-PURs) via the reaction of bis-cyclic carbonates and bis-amines have been developed even under mild conditions.(*5, 9-13*) Another alternative approach is chemical recycling through depolymerizing PURs into recyclable monomers. Unlike other plastics (e.g., PET, polyolefins), PURs are seldom recycled due to their complex structure and crosslinked thermoset nature.(*14*) Their depolymerization typically requires harsh conditions (180–250 °C, 50 bar), and the resulting diamines must be converted to diisocyanates or bis-carbonates to re-enter the production cycle. Currently, recycling relies on glycolysis (feedstock recycling) (*15, 16*) and grinding (mechanical recycling), both of which are energy-intensive and mostly yield polyols for downcycling.(*14, 17-19*) An appealing yet underexplored strategy for depolymerizing PURs is methanolysis. Although it requires high temperatures and supercritical methanol, it produces dimethyl carbamates and polyols that can be directly repolymerized into PURs—unlike glycolysis-derived monomers.(*20*)

Enzymatic depolymerization offers a more sustainable alternative. Evolved to operate under mild conditions, enzymes provide high selectivity and simplified purification. In polyesters like PET, enzymatic recycling has seen breakthroughs, (*21-26*) but progress is rather limited for PURs. These polymers contain a complex mix of covalent bonds (ether, ester, urethane), which makes them harder to degrade than polyesters like PET, which consist solely of ester bonds. Most reported enzymatic PUR depolymerizations are limited to polyester-based PURs and require long incubation periods (>10 days), primarily hydrolyzing ester domains while leaving urethane bonds untouched (**Scheme 1A**).(*27-33*) Enzymatic activity on polyether PURs is generally negligible. While urethane-bond-cleaving activity has been observed,(*33*) urethane bonds, especially in the hard segments of PURs, remain hard to access.

Recently, a new family of enzymes with urethanase activity was identified from a metagenomic library sourced from PUR-contaminated soil. The most promising candidate, UMG-2,(*34*) was engineered for higher activity via semi-rational mutagenesis.(*35*) So far, its activity has only been demonstrated on dicarbamates derived from the glycolysis of PUR foams. These enzymes have enabled a chemoenzymatic process, where polyols are recovered chemically, while diamines are released enzymatically from dicarbamates (**Scheme 1B**). Yet, the detailed enzymatic mechanism remains unclear.(*35, 36*) Despite these advances, direct enzymatic depolymerization of polyether-based PUR thermosets remains elusive. In addition to the lack of efficient urethanases, depolymerizing thermoset PURs faces mass transport limitations.

Unlike thermoplastics like PET, thermoset PURs are water-insoluble and remain in solid form during hydrolysis, making enzymatic access difficult. Enzymes thus operate in biphasic systems, with the PUR as a solid substrate and enzymes in the liquid phase. To address plastic solubility issues, organic solvents are used to enhance the swelling of plastic materials, thus improving the catalytic depolymerization processes.(*37*) However, enzymes typically exhibit low performance under these conditions. To address such challenges in biocatalysis, reaction media engineering plays a crucial role by improving the solubility or accessibility of substrates.

Since the 1980s, Klibanov and others have shown that enzymes can function in organic solvents, enabling reactions not possible in water.(*38-42*) This led to growing interest in non-conventional solvents like ionic liquids, supercritical fluids, and deep eutectic solvents.(*43*) While promising in applied biocatalysis, these systems remain underexplored for plastic depolymerization. Among the few examples reported, lipase B from *Candida antarctica* (CALB) has successfully hydrolyzed aliphatic polyesters like PLA and PCL in ionic liquids and organic solvents,(*44*,*45*) which helps enzymes to access hydrophobic polymers. Interestingly, a combination of CALB and urease partially hydrolyzed bis(2-methoxyethyl) dicarbamates in a ternary solvent system (solketal, ionic liquid, and water).(*33*) However, these enzymes were not tested directly on PUR foams. Alternatively, solvolysis using organic solvents is attractive, as solvents like alcohols can act as both reaction media and nucleophiles, enhancing catalyst solubility and foam penetration. However, enzyme-catalyzed transcarbamoylation remains unexplored for polyurethane depolymerization, even though lipases are well-established catalysts for the transesterification of oils in biodiesel production. (*46-48*)

In this work, we screened a variety of hydrolases (lipases, proteases, cutinases, urethanases) for their ability to catalyze the transcarbamoylation of PUR thermosets in primary alcohols under mild conditions (**Scheme 1C**). Initial tests on model *p*-nitrophenyl *N*-benzyl carbamate (PNPBC) showed that lipases from *Rhizopus oryzae* (ROL) and *Thermomyces lanuginosus* (TLL) were promising biocatalysts for urethane bond transcarbamoylation. These findings were supported by QM/MM molecular dynamics (MD) simulations. After evaluating various alcohols, we performed alcoholysis of both isocyanate- and non-isocyanate-based PUR thermosets using TLL in methanol and ROL in ethanol. Analysis of the degraded foams and reaction mixtures revealed plastic breakdown and release of alkyl dicarbamates and polyols, which could be potentially repolymerized under basic catalysis. The polyols were indeed isolated and used to manufacture a recycled foam. Thus, we report the first use of lipases to depolymerize PURs via transcarbamoylation, offering a milder alternative to traditional recycling and producing building blocks directly usable in new polymer synthesis.

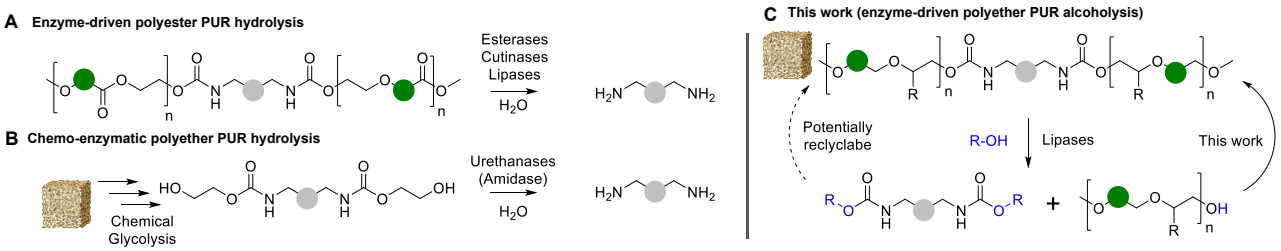

Scheme 1. Biocatalytic transformation of polyurethanes (PUR). **(A)** Enzyme hydrolysis of polyesters PUR.(*27-33*) **(B)** Chemo-enzymatic transformation of polyether PUR into diamines through glycol dicarbamates intermediates.(34-36) **(C)** Alcoholysis of polyether PUR foams catalyzed by lipases as described in this work.

Our strategy differs fundamentally from prior enzymatic depolymerization efforts by using alcohols as both solvents and nucleophiles, enabling a distinct catalytic mechanism.(*25, 49*)

RESULTS and DISCUSSION

Enzyme screening for alcoholysis of urethane bonds

To investigate the enzymatic alcoholysis of urethane bonds, we focused on hydrolases as the potential enzyme family capable of performing this reaction. We first built up a phylogenetic tree using 283 sequences of known hydrolases able to hydrolyze ester and amide bonds from the UniProt database (**Figure S1**). From this tree, we selected ten enzymes from different hydrolase subclasses that represent a good coverage of both sequence and functional diversity, including lipases, cutinases, proteases, and a recently identified urethanase (**Figure 1A** and **Table S1**). As the model reaction, we selected the alcoholysis of PNPBC (**Figure S2**) in the presence of methanol with low water content (0-13%) for 7 hours at 25 °C. Under these conditions, a transcarbamoylation reaction occurs, thermodynamically driven by the release of *p*-nitrophenol as a leaving group (**Figure 1B**).

Unlike in methanol, PNPBC is poorly soluble in water, which makes it a suitable substrate for alcoholysis, as spontaneous hydrolysis is minimized. While *p*-nitrophenol derivatives are widely used for hydrolase screening,(*50-52*) they are less commonly employed for alcoholysis studies. The reaction product, methyl *N*-benzylcarbamate, was detected by ^{1}H-NMR and UPLC-MS (**Figure S3-S4A**).

In the methanolysis screening, lipases showed the highest titers of methyl *N*-benzylcarbamate (**Figure 1C**). Among them, lipases from *Thermomyces lanuginosus* (TLL) and *Rhizopus oryzae* (ROL) exhibited the highest specific activity (0.6 mM h^{-1} mg^{-1}). Next, we assessed the substrate scope of these two lipases in the alcoholysis of PNPBC, analyzing the resulting alkyl carbamates through UPLC-MS (**Figure S4**). As shown in **Figure 1C**, both enzymes accept different alcohols but prefer the shortest, like methanol. While both enzymes perform similarly in methanol, ROL outperforms TLL for ethanolysis. Although methanolysis is particularly relevant, as methyl carbamates are ready-to-use monomers for polymerizing free-isocyanate PURs,(*53*) the formation of ethyl carbamates in ethanolysis is also attractive. The performance of these two lipases in alcoholysis reactions for transcarbamoylation of urethane bonds is supported by their tolerance to methanol and their ability to catalyze solvent-free methanolysis of fatty oils, resulting in high yields of methyl and ethyl fatty esters

Then, we studied the stability of TLL and ROL in alcohols at different temperatures to assess their capacity to perform PUR depolymerization during longer times at higher temperatures. The intrinsic enzyme stability in either water or alcohol (MeOH and EtOH) was assessed by incubating the same enzyme concentration with alcohol but without PNPBC at either 25 or 50 ºC for 24 hours. After this incubation, the esterase activity of the enzyme was measured using a colorimetric assay under the optimal conditions (25 mM phosphate buffer at pH 7 and 25 ºC). **Figure 1D** shows the specific activity of both lipases before and after incubation with and without the corresponding alcohol. Both enzymes retained high specific activity upon their incubation in ethanol. Surprisingly, the specific activity after incubation in EtOH at 50 °C was higher than that after incubation in water at the same temperature. Suggesting that these lipases are stabilized by high ethanol concentration through restricting protein conformation dynamics.(*58*) In contrast, the specific activity of both enzymes decreased drastically in the presence of methanol. This inactivation was more dramatic when the enzyme was incubated at 50 ºC, where the residual specific activity was lower than 1% of

the specific activity measured for the non-incubated preparation. The activity results are through transesterification.(*54-57*) supported by the folding stability (Melting temperature (T_M)) of both lipases upon 24 h incubation with the two alcohols at different temperatures (**Figure S5, Table S2**). While both enzymes are thermodynamically stable in EtOH, the methanol dramatically affected the folding stability of both enzymes at high temperatures. Due to its smaller size, methanol penetrates the hydrophobic core of proteins more efficiently than larger alcohols (i.e, ethanol), disrupting protein structural integrity. (*59-61*) However, at milder temperatures (30 ºC), TLL exhibited higher folding stability in MeOH than ROL, likely due to the higher thermostability of the former enzyme.(*62*) Based on these results, we selected two lipases: TLL specifically for the methanolysis, and ROL for the ethanolysis of aromatic polyurethanes

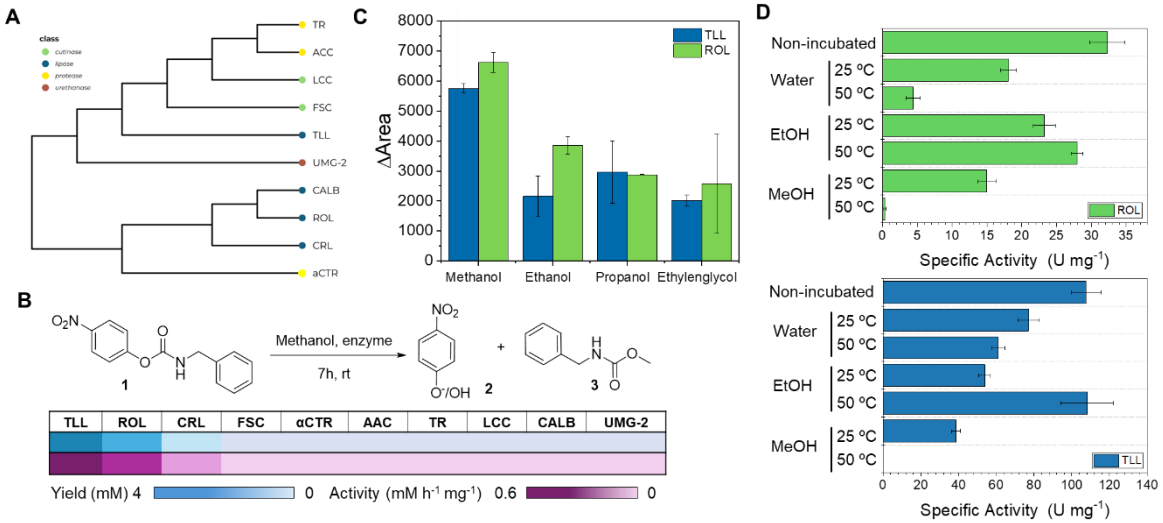

Figure 1: Enzyme screening using a urethane model substrate (*p*-nitrophenol N-benzyl carbamate; PNBC; (**1**). **(A)** Selected hydrolases organized by their sequence-structure similarity according to a phylogenetic analysis (see **Figure S1**). The selected enzymes for the screening are: i) lipases from *Thermomyces lanuginosus* (TLL), from *Rhizopus oryzae* (ROL), from *Candida rugosa* (CRL), and from *Candida antartica* (lipase B; CALB), the proteases trypsin (TR) and α-chymotrypsin (αCTR) from bovine pancreas, the cutinases from *Fusarium solani* (FSC), from *Arxula adeninivorans* (AAC), and from leaf and branch compost (LCC), and the metagenomic-derived urethanase (UMG-2). **(B)** Scheme of methanolysis reaction (top) and heatmap of screening results (bottom) using PNBC as substrate in the presence of methanol as alcoholysis reagent. Methanolysis efficiency is represented as the chromatographic yield of (blue) and enzyme activity (purple) toward methyl N-benzyl carbamate (**3**) after 7 h at room temperature (rt ~ 25 ºC). **(C)** Alcoholysis reactions of PNPBC (**1**) with different alcohols catalyzed by either TLL or ROL in 24 h at 25ºC. The products were detected by HPLC, and the magnitude of alcoholysis was assessed by quantifying the UV-Vis areas of the alkyl *N*-benzylcarbamates. **(D)** Alcohol stability test of TLL and ROL. Both enzymes were incubated either in water, ethanol (EtOH), or methanol (MeOH) at 25 or 50 ºC for 24 h.

Then, we studied the stability of TLL and ROL in alcohols at different temperatures to assess their capacity to perform PUR depolymerization during longer times at higher temperatures. The intrinsic enzyme stability in either water or alcohol (MeOH and EtOH) was assessed by incubating the same enzyme concentration with alcohol but without PNPBC at either 25 or 50 ºC for 24 hours. After this incubation, the esterase activity of the enzyme was measured

using a colorimetric assay under the optimal conditions (50 mM phosphate buffer at pH 7 and 25 ºC). **Figure 1D** shows the specific activity of both lipases before and after incubation with and without the corresponding alcohol. Both enzymes retained high specific activity upon their incubation in ethanol. Surprisingly, the specific activity after incubation in EtOH at 50 °C was higher than that after incubation in water at the same temperature. Suggesting that these lipases are stabilized by high ethanol concentration through restricting protein conformation dynamics.(*58*) In contrast, the specific activity of both enzymes decreased drastically in the presence of methanol. This inactivation was more dramatic when the enzyme was incubated at 50 ºC, where the residual specific activity was lower than 1% of the specific activity measured for the non-incubated preparation. The activity results are supported by the folding stability (Melting temperature (T_m)) of both lipases upon 24 h incubation with the two alcohols at different temperatures (**Figure S5, Table S2**). While both enzymes are thermodynamically stable in EtOH, the methanol dramatically affected the folding stability of both enzymes at high temperatures. Due to its smaller size, methanol penetrates the hydrophobic core of proteins more efficiently than larger alcohols (i.e, ethanol), disrupting protein structural integrity. However, at milder temperatures (30 ºC), TLL exhibited higher folding stability in MeOH than ROL, likely due to the higher thermostability of the former enzyme.(*62*) Based on these results, we selected two lipases: TLL specifically for the methanolysis, and ROL for the ethanolysis of aromatic polyurethanes.

Molecular dynamics (MD) and quantum mechanics/molecular mechanics (QM/MM) simulations of TLL in the methanolysis reaction of a model aromatic urethane.

To better understand the lipase-driven alcoholysis of urethane bonds, we explored the molecular mechanism of TLL in methanolysis reactions through molecular dynamics (MD) simulations, with classical and hybrid quantum mechanics/ molecular mechanics (QM/MM) potentials. These computational studies were performed with the urethane compound used in the enzyme screening, PNPBC (see supplementary material, **figures M1-M4** and **table M1**). We first analyzed the behavior of TLL when solvated in methanol. As in most lipases, TLL exhibits shielding of the catalytic site from the external environment by a lid region (residues 84–96) that covers the catalytic triad (Ser146, His258, and Asp201).(*63*) Keeping in mind our interest in docking the PNPBC into the active site of TLL, we used the X-ray solved crystal structure of TLL in the open conformation (PDB ID 1DT3).(*63*)

After setting up enzyme solvation in a box of methanol molecules (see Supporting Information for details), MD simulations revealed the stability of the open conformation, resulting in a structure with the active site fully exposed to the solvent. PNPBC was then docked into the TLL active site. Among the most favorable binding poses, two distinct orientations were identified—pose 1 and pose 2—characterized by the orientation of the nitro group either pointing inward the cavity or outward from the binding pocket of TLL (**Figure 2A**). Interestingly, replicas of MD simulations reveal that while pose 2 stays in the active site, the substrate is spontaneously released from the active site when starting from pose 1 (**Figures 2A and S6-S8**). Moreover, geometrical analysis of the replicas in pose 2 shows how the substrate adopts a reactive conformation to attack the urethane bond of PNPBC (**Figure S9-S12**). Based on these results, we suggest that pose 2 is the conformation PNPBC adopts in the active site, showing an optimal orientation regarding the catalytic residues, Ser146 and His258. This suggestion is supported by the enzyme-substrate interaction analysis (**Figures 2B and S13**).

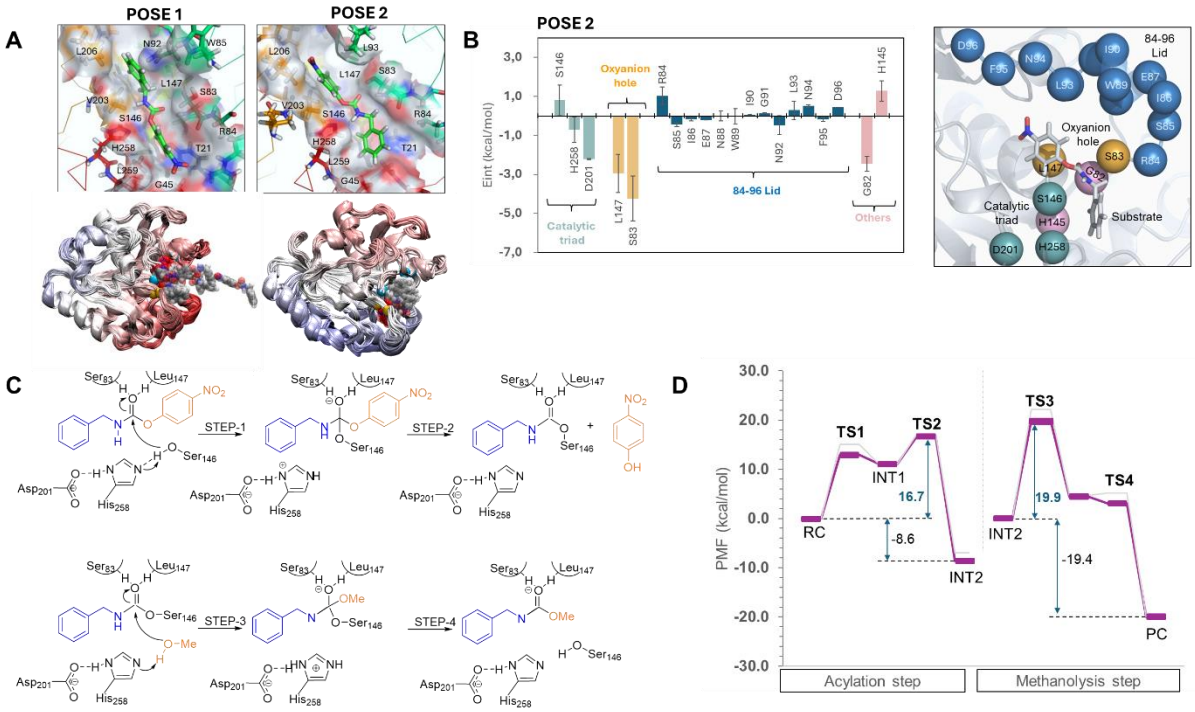

Figure 2. Computational results of PNPBC methanolysis catalyzed by TLL. **(A)** Structures of two poses of PNPBC in the TLL active site as derived from molecular dynamics (MD). Top images: all-atom interaction from the TLL binding pocket and PNPBC in the two poses. Bottom images: cartoon representation of MD snapshots of the enzyme-substrate complex in the two poses obtained along the MD. The enzymes are colored from more flexible (red) to less flexible regions (blue). **(B)** Interaction energies (Eint) (left) and residue contacts (right) between the TLL active site and PNPBC. The different amino acids forming the catalytic triad (turquoise), the lid (blue), the oxyanion hole (yellow), and other contacts are colored in both the bar plot and the active site representation. Standard deviations are shown as error bars. **(C)** Scheme of the stepwise reaction mechanism. **(D)** QM/MM free energy profile for the methanolysis of PNBC catalyzed by TLL.

Moreover, geometrical analysis of the replicas in pose 2 shows how the substrate adopts a reactive conformation to attack the urethane bond of PNBC (**Figure S9-S12**). Based on these results, we suggest that pose 2 is the conformation PNPBC adopts in the active site, showing an optimal orientation regarding the catalytic residues, Ser146 and His 258. This suggestion is supported by the enzyme-substrate interaction analysis (**Figures 2B and S13**).

Consequently, we explored the chemical steps to calculate the reaction profile of the PNPBC methanolysis starting from the equilibrated enzyme: substrate complex in pose 2 (**Figure S8**). We assumed that the TLL-driven methanolysis of PNPBC occurs through the conventional two-step pathway for hydrolases. As illustrated by **Figure 2C**, this pathway starts with an acylation step followed by the deacylation (or methanolysis) step. According to QM/MM calculations at 298 K (**Figures 2D and S14, and Table S3**), both the acylation and the deacylation steps are exergonic. This reaction profile is consistent with an enzyme-catalyzed process. From a kinetic perspective, we found that the rate-limiting step of PNPBC methanoyls is the diacylation step that requires the activation of a MeOH molecule and its nucleophilic attack on the carbonyl carbon of the acyl-enzyme intermediate. This step presents an activation free energy of 19.9 kcal·mol^{-1}. Remarkably, our computational results

predict an activation free energy that closely matches the experimental catalytic constant (k_{cat} = 0.38 ± 0.27 s^{-1}, **Figure S15**), corresponding to an energy barrier of 18.2 kcal·mol^{-1} within the framework of transition state theory and under comparable reaction conditions (100% methanol). All in all, the computational studies supported by the experimental data confirm the capacity of TLL to catalyze the methanolysis of urethane bonds in model substrates like PNPBC.

Lipase-driven alcoholysis of polyether polyurethanes.
As polyether PURs are largely represented in commercial PUR-based plastics used as adhesives, glue, coating, foams, and elastomers, we selected them to assess the depolymerization potential of lipase-driven alcoholysis. In this study, we constructed a linear low molecular weight PUR polymer model that contains aromatic monomers in the hard segment formed by the polymerization of toluene diisocyanates (TDI) and polyether polyols based on 1,2-propanodiol and capped with 1,4-butanodiol (TDI-PUR) (**Figure 3A**).

TDI-PUR polymer (Mw: 36500 g mol^{-1}) was incubated with ROL and ethanol, and with TLL with methanol in 13% water. Despite the low stability of both enzymes in methanol at high temperature, we raised the reaction temperature to 50 ºC to overcome the thermodynamic barriers of depolymerization reactions.(*64*) After 7 days of incubation at 50 ºC, the reaction crude was extracted with dichloromethane to separate the polymers from the enzymes, and the organic phase was analyzed by gel-permeation chromatography to observe changes in the molecular weight of the polymer (**Figures 3B-C and Table S4**). In the presence of methanol, TLL decreased the polymer molecular weight by two times. Likewise, ROL reduces the polymer molecular weight of TDI-PUR polymer three times when incubated with ethanol. Moreover, ROL-driven ethanolysis resulted in a 36% decrease in polymer density, supporting the enzymatic degradation of this polymer. These results indicate that both lipases break down the polymer chains of TDI-PUR using short primary alcohols as solvents.

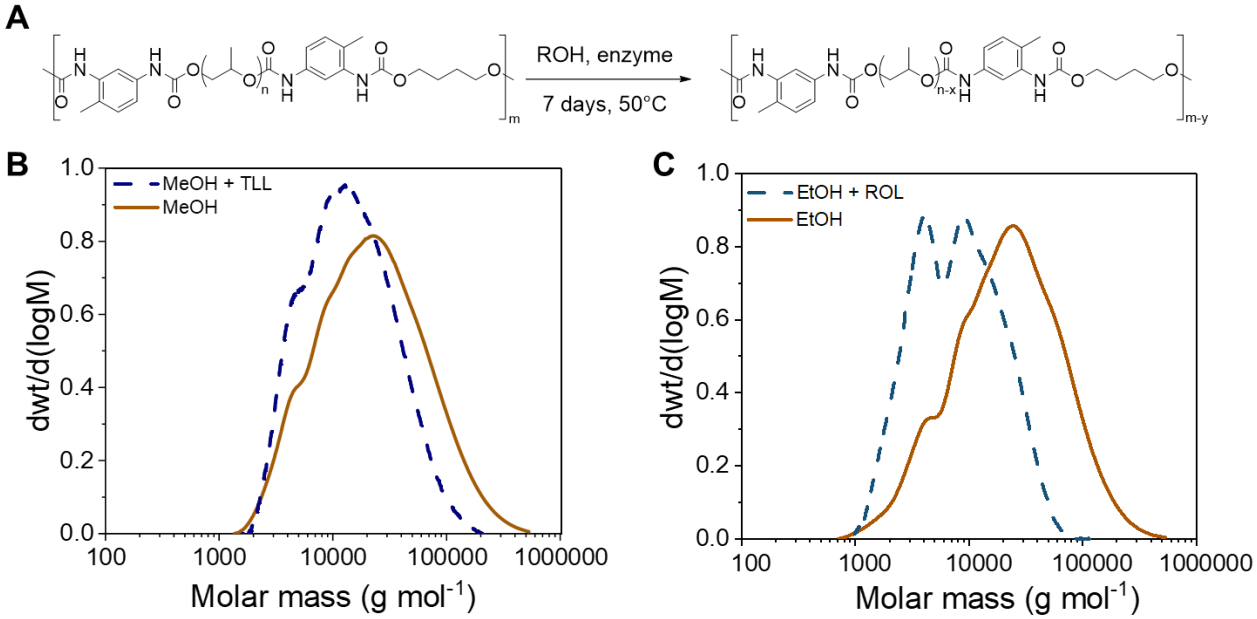

Figure 3: Enzymatic alcoholysis of a linear thermoplastic polyether polyurethane (TDI-PUR). **(A)** Alcoholysis reaction scheme and conditions. **(B, C)** Gel permeation chromatography (GPC) chromatograms of TDI-PUR incubated in methanol **(B)** and ethanol **(C)** at 50 ºC with (blue dashed line) and without (solid brown line) the corresponding lipase. 1 mg ml^{--1} of either TLL or ROL was used for the methanolysis and ethanolysis, respectively, using 25 mg ml^{-1} of PU-TDI.

TDI-PUR polymer (Mw: 36500 g mol^{-1}) was incubated with ROL and ethanol, and with TLL with methanol in 13% water. Despite the low stability of both enzymes in methanol at high temperature, we raised the reaction temperature to 50 ºC to overcome the thermodynamic barriers of depolymerization reactions.(*64*) After 7 days of incubation at 50 ºC, the reaction crude was extracted with dichloromethane to separate the polymers from the enzymes, and the organic phase was analyzed by gel-permeation chromatography (GPC) to observe changes in the molecular weight of the polymer (**Figures 3B-C and Table S4**). In the presence of methanol, TLL decreased the polymer molecular weight by two times. Likewise, ROL reduces the polymer molecular weight of TDI-PUR polymer three times when incubated with ethanol. Moreover, ROL-driven ethanolysis resulted in a 36% decrease in polymer density, supporting the enzymatic degradation of this polymer. These results indicate that both lipases break down the polymer chains of TDI-PUR using short primary alcohols as solvents.
Encouraged by these results, we applied the two lipases to the alcoholysis of synthetic TDI-PUR thermoset foams (**Figure S16**). These foams are among the most commercially prevalent PUR materials, but their recycling remains challenging due to their complex and crosslinked composition. We hypothesize that the hard segment of TDI-PUR foams is targeted by the lipases through a transcarbamoylation reaction. In this reaction, the urethane bond is selectively cleaved at the carbon–oxygen (C–O) bond of the carbamate group (–NH–CO–O–), rather than at the carbon–nitrogen (C–N) bond. This cleavage occurs through nucleophilic attack by alcohol molecules, resulting in the formation of alkyl dicarbamates (**Figures S17-S18**).

To prove this hypothesis, we incubated the TDI-PUR foams with TLL in methanol and with ROL in ethanol for 7 days at 50 ºC. After biocatalytic alcoholysis, we extracted the reaction media and washed the foams with an excess of distilled water to remove reaction debris. The washed foams were analyzed by electron microscopy (SEM) to visualize the structural alterations promoted by the enzyme-driven alcoholysis. First, we observed that the foams were more deteriorated than those incubated with the corresponding alcohol in the absence of the enzymes (blank) (**Figure 4A and 4B**). When comparing the two samples, TDI-PUR foam treated with TLL in methanolysis underwent a more significant structure collapse than the same treated with ROL in ethanolysis. SEM images illustrate the eroding action of TLL on the surface of TDI-PUR foams in the presence of methanol, losing their microporous structures. **Figures 4C** and **4D** show how the larger macropores collapse into more compacted structures upon methanolysis, with less structural modification upon ethanolysis. This collapse suggests that the crosslinking network of the foam was weakened due to the cleavage of urethane bonds in the foam network.

In parallel, we analyzed the enzymatically treated foams by ATR-FTIR **(Figures 4E and 4F)**. In methanolysis, the FTIR spectrum reveals a broad band in the 3400–3300 cm^{-1} range, attributed to O-H and N-H stretching associated with free hydroxyl or amine groups.(*65, 66*) Compared to the blank, this band is more intense in enzyme-treated samples, suggesting a higher concentration of free hydroxyl and/or amine groups on the foam surface. However, the band at 1533 cm^{-1}, associated with the NH amide in urethane bonds,(*31*) remains similar in both enzyme-treated samples and the blank. Consequently, the intensity ratio of the 3295 cm^{-1} and 1533 cm^{-1} bands increases significantly between the blank and enzyme-treated samples (**Figure S19A**). In contrast, when we analyzed the intensity ratio between the stretching of the ether bonds (1096 cm^{-1}) and that of the NH amide of urethane bonds (1533 cm^{-1}),(*67*) we found a lower ratio in enzyme-treated samples compared to the blank,

suggesting the disappearance of ether bonds from the foam surface (**Figure S19B**). Based on ATR-FTIR data, we propose that methanolysis preserves urethane bonds in the hard segments as methyl carbamates, while cleaving polyether chains from the soft segments, releasing free hydroxyl groups at the surface of the foam. The presence of more free O–H groups and fewer ether bonds suggests that polyols were released from urethane linkages via enzyme-driven alcoholysis, leading to reduced crosslinking in the PU chains and contributing to the observed foam collapse. Similarly, the FTIR spectrum of ethanolysis samples shows an increase in the 3400–3300 cm^{-1} band. Yet, such an increase was less pronounced than in methanolysis, resulting in a lower 3295 cm^{-1}/1533 cm^{-1} ratio (**Figure S19A**). However, the ratio between ether and urethane bonds (1093 cm^{-1}/1533 cm^{-1}) remained constant after the enzyme treatment (**Figure S19B**), suggesting a limited release of polyols to the reaction media. This semi-quantitative analysis indicates that methanolysis is more efficient than ethanolysis, which aligns with the less eroded samples observed in ROL-driven ethanolysis according to SEM analysis (**Figure 4C and 4D**). These results suggest that methanol acts as a better solvent and greater nucleophile for TLL,(*68*), facilitating enzyme access to the inner surfaces of the porous foams and thus enzyme catalysis.

At this point, it was difficult to unambiguously conclude that alcoholysis is driving the PUR dismantling because enzyme preparations contained water (up to 13% in the case of TLL). This water could trigger the hydrolysis of the polyurethane chains, competing with the target alcoholysis reaction. To understand this, we decided to incubate the TDI-PUR foams with the TLL in full aqueous media using distilled water as the solvent for 7 days at 50 ºC (**Figure S20**). Under these conditions, visual inspection and SEM analysis showed that enzyme hydrolysis negligibly affected the macroscopic aspect of the foam. By studying the TLL-driven methanolysis reaction under varying water contents, we observed that lower water content led to a higher signal ratio of hydroxyl to urethane groups and, correspondingly, a lower signal ratio of ether to urethane bonds (**Figure S21**). These trends indicate that water minimizes the release of polyols from the foam, and consequently, the content of the free hydroxyl groups at the foam surface. Therefore, 13-17% became the optimal water content to maximize the alcoholysis of urethane bonds. These results evidence the key role of water in this biotransformation, as an excess competes with the alcoholysis and hampers the enzyme diffusion through the surface of the PUR foam.

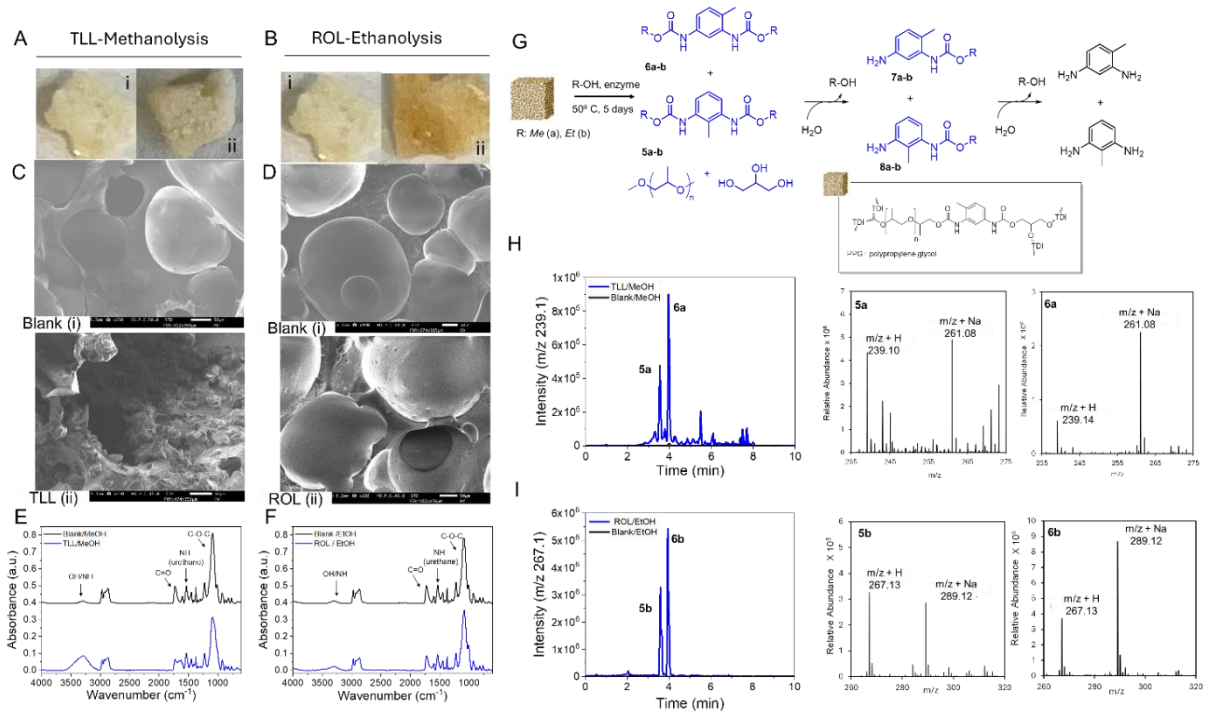

Figure 4: Alcoholysis reactions of TDI-PUR foam catalyzed by TLL (**A, C, E**, and **H**) and ROL (**B, D, F**, and **I**) in methanol and ethanol, respectively. Optical (**A** and **B**) and SEM images (**C** and **D**) of foams after 7 days incubation at 50 ºC in the corresponding alcohol (**A** and **C** for methanol, **B** and **D** for ethanol) without (blank (i)) and with (ii) the corresponding lipase. ATR-FTIR spectra of the resulting foams after methanolysis (**E**) and ethanolysis (**F**) conditions in the presence (blue) and in the absence (black) of the corresponding enzyme. **(G)** Hypothetical reaction scheme if hydrolysis occurs sequentially to alcoholysis, with detected products in blue. (**H, I**) UPLC-MS traces (left) and MS spectra (right) of reaction crudes extracted with organic solvents upon 7 days of methanolysis (**H**) and ethanolysis (**I**). Blue and black traces represent reaction with and without the corresponding lipase, respectively.

In parallel, we recovered the reaction crude through gravity filtration, and the liquid phase was centrifuged. As a result, we obtained a white paste that was soluble in tetrahydrofuran. MALDI-TOF analysis of that paste revealed the presence of a polymeric molecule with 58 Da units and an average molecular weight of approximately 3.5 kDa (**Figure S22**). These technical properties match the original polyols used for the synthesis of this TDI-PUR foam.(*69*) Thus, the presence of polyether polyols in the reaction crude proved their release during the enzymatic depolymerization process. Furthermore, the release of polyols is consistent with the ATR-FTIR data acquired with the enzyme-treated foam in methanolysis, which showed a decline in polyol content in the foam after enzyme treatment (**Figure S19A**).

To confirm that both TLL and ROL were able to perform the alcoholysis of TDI-PUR foams instead of hydrolysis, we also analyzed the liquid phases resulting from the alcoholysis reaction upon centrifugation of reaction crudes. These liquid samples were then extracted through liquid-liquid phase extraction and evaporated. Finally, the samples were dissolved in acetonitrile and analyzed by UPLC-MS. Retention times and mass spectrometry spectra were compared to the corresponding standards chemically synthesized (**Figure S17-S18**), to confirm the presence of dicarbamates upon enzyme action. In TLL-driven methanolysis, we could identify the two isomers (2,4-diamino-methyltoluene and 2,6-diamino-methyltoluene) of the methyl dicarbamates **(Figure 4G; 5a-6a**) resulting from the alcoholysis of TDI-PUR foams **(Figure 4H)**. To note, the proportion of these two isomers was similar to

the isomer composition of this polymer in the PUR foams.(*70*) Increasing the water content in the methanolysis reaction decreased the production of the methyl dicarbamates (**Figure S23)**. Similarly, when we analyzed the ethanolysis reaction crude obtained from the foam samples incubated with ROL, we could also identify the ethyl dicarbamates (**Figure 4G; 5b-6b**) by UPLC-MS (**Figure 4I**). In both alcoholysis reactions, we could also identify alkyl monocarbamates (**Figure 4G; 7a-b and 8a-b, and S24**). However, diamines were not detected in the reaction bulk. Due to the presence of these alkyl monocarbamates in the reaction liquid phase, we propose a sequential mechanism in which the lipases first use primary alcohols to cleave the urethane bonds from the most superficial polymer chains of the foams. This yields alkyl dicarbamates, which may be subsequently hydrolyzed in the reaction medium by the enzymes, generating partially hydrolyzed monoalkyl carbamates (**Figure 4G**). We suggest that the water required for this partial hydrolysis originates from the enzyme preparations, supporting the idea that once the carbamates are released from the foams, they can be hydrolyzed in the liquid phase. However, the available water was insufficient to wet the TDI-PUR foam for direct hydrolysis and not enough to fully hydrolyze the carbamate intermediates in the liquid phase. Therefore, we propose that these lipases depolymerize TDI-PUR foams through catalyzing their alcoholysis at the solid–liquid interface, followed by the partial hydrolysis of released monomers in the liquid phase. When foams resulting from the enzyme treatment were analyzed by thermal gravimetry (TGA, **Figure S25**) and differential scanning calorimetry (DSC, **Figure S26**), we found that both enzyme-driven alcoholysis changes the polymer composition. Specifically, the lower T95% reveals the presence of shorter polymers in the treated foams.

Encouraged by the detection of polyols and methyl dicarbamates upon TLL-driven methanolysis, we scaled this depolymerization reaction up to 3 grams of foam in 100 mL of reaction mixture. After the workup (see methods), we isolated a solid paste that was dissolved in chloroform and analyzed by ^{1}H- and ^{13}C-NMR, confirming the presence of polyol PPG (**Figures 5A-B, Figure S27-29**). Then, the methanol miscible fraction was dried, and the solid was extracted with a chloroform/water mix. The organic phase was analyzed by NMR, identifying glycerol (**Figure S30-32**) and aromatic compounds (**Figure S33-34**), yet pure methyl dicarbamates could not be isolated. Therefore, the enzyme-driven methanolysis process releases polyols from the foam that are readily recovered upon filtration of the depolymerization debris, yet the isolation of methyl dicarbamates failed. Further optimization of workup is needed to isolate the methyl dicarbamate compounds for their repolymerization. Next, we fabricated a new TDI-PUR foam containing 50% of enzymatically recycled polyols by reacting them with TDI-isocyanate and virgin polyols, using 1,4-diazabicyclo[2.2.2]octane (DABCO) as a catalyst. The resulting PUR foam was similar to the virgin one, both at macroscopic and microscopic levels (**Figures 5C-D**). Moreover, the IR-fingerprint of the recycled foam was very similar to the virgin one (**Figure 5E**). Through the enzymatic deterioration of TDI-PUR foams in methanol, we pioneer a closed-loop recycling of polyols using biological methods. This approach represents a breakthrough in biocatalysis, enabling the direct recycling of polyether PUR-based thermosets without any upstream chemical processing.

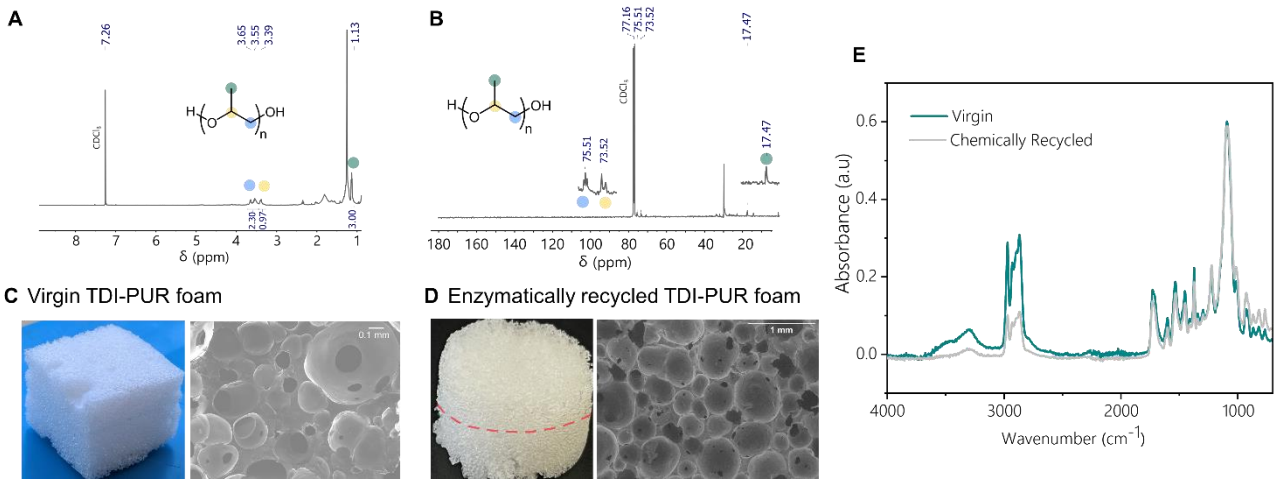

Figure 5. Closed-loop TDI-PUR recycling process via enzymatic methanolysis. (**A**) ^{1}H NMR and (**B**) ^{13}C NMR spectra of the recycled polypropylene glycol (PPG) isolated from enzyme TDI-PUR foam depolymerization, confirming its chemical structure after recovery. (**C, D**) Photographs (left) and SEM images (right) of the virgin (**C**) and enzymatically recycled (**D**) TDI-PUR foams. Foams present a uniform, closed-cell morphology in both virgin and enzymatically recycled foams. (**E**) ATR-FTIR spectra comparing the recycled PPG-based foam with the same virgin foam formulation.

Scope of lipase-driven alcoholysis toward polyether-PUR foams of different composition

Encouraged by the results for the alcoholysis of TDI-PUR foams, we decided to expand the scope of this biocatalytic depolymerization to non-isocyanate PUR foams based on aromatic diamines ([3-(aminomethyl)phenyl]methanamine) and aliphatic triamines (*N*', *N*'-bis(2-aminoethyl)ethane-1,2-diamine) formulated in a molar ratio 1:2 using aliphatic carbonates as chain extenders (NI-PUR). Unlike TDI-PUR foams, NI-PUR foams display free hydroxyl groups adjacent to the carbamate groups, increasing the hydrophilicity of the polymers and their intramolecular network through H-bond formation (**Figure S35**). Furthermore, carbamates are made of a mixture of aromatic and aliphatic diamines, unlike TDI-PURs, which are composed only of toluene-derived diamines. Therefore, NI-PUR foams present different mechanical and physicochemical properties compared to the TDI-PUR foams studied above. These differences suggest that biochemical depolymerization based on lipase-driven alcoholysis may perform differently than with conventional isocyanate-based PUR. To test this hypothesis, we incubated NI-PUR samples with either TLL in methanol or ROL in ethanol under similar conditions to those described for the enzymatic alcoholysis of TDI-PURs (50 ^{o}C, but for 5 days). After biocatalytic alcoholysis, the foams were washed and analyzed by SEM and ATR-FTIR, while the reaction crudes were analyzed by UPLC-MS after workup (**Figure 6**). Furthermore, the enzyme-treated NI-PUR foams were analyzed by TGA (**Figure S25**) and DSC (**Figure S36**). Altogether, these data evidence that both lipases erode NI-PUR foams in the presence of both alcohols.

Our first observation was that the NI-PUR foams were significantly more deteriorated than the negative controls (without enzyme), but also than the TDI-PUR foams subjected to biocatalytic alcoholysis (**Figures 6A-B**). When comparing the two samples, the structure of NI-PUR foams treated with both TLL in methanolysis and ROL in ethanolysis was completely collapsed. Specifically, SEM images illustrate the action of lipases eroding the surface of NI-PUR foams in the presence of the two alcohols, leading to the collapse of larger macropores into compacted structures with reduced porosity (**Figure 6C-D**). This collapse suggests that the crosslinking network of the foam was weakened due to the breaking of urethane bonds in the foam. UPLC-MS confirmed that both TLL and ROL were able to perform the

alcoholysis of NI-PUR foams as proposed (**Figure 6G**). In TLL-driven methanolysis, we identified the aromatic methyl dicarbamate (methyl *N*-[[3-[(methoxycarbonylamino)methyl]phenyl]methyl]carbamate, (**Figure 6G; 9a** and **Figure 6H**). In contrast, when the same foam was incubated with ROL and ethanol, we found no aromatic dicarbamates but aliphatic tricarbamates resulting from the ethanolysis of the urethane bonds formed with the aliphatic triamine (**Figure 6G; 10b** and **Figure 6I**). Moreover, the ethyl-monocarbamate was detected (**Figure S37**), suggesting the hydrolysis of carbamates upon the transcarbamoylation reaction (**Figure 6G**), following a similar sequential mechanism as the one proposed for TDI-PUR foams. The physicochemical properties of the enzyme-treated NI-PUR foams were altered compared to their untreated counterpart, as shown by TGA **(Figure S26**) and DSC (**Figure S37**) analyses. Specifically, the lower T95% reveals the presence of shorter polymers in the enzymatically treated foams.

Our first observation was that the NI-PUR foams were significantly more deteriorated than the negative controls (without enzyme), but also than the TDI-PUR foams subjected to biocatalytic alcoholysis (**Figures 6A-B**). When comparing the two samples, the structure of NI-PUR foams treated with both TLL in methanolysis and ROL in ethanolysis was completely collapsed. Specifically, SEM images illustrate the action of lipases eroding the surface of NI-PUR foams in the presence of the two alcohols, leading to the collapse of larger macropores into compacted structures with reduced porosity (**Figure 6C-D**). This collapse suggests that the crosslinking network of the foam was weakened due to the breaking of urethane bonds in the foam. UPLC-MS confirmed that both TLL and ROL were able to perform the alcoholysis of NI-PUR foams as proposed (**Figure 6G**). In TLL-driven methanolysis, we identified the aromatic methyl dicarbamate (methyl*N*-[[3-[(methoxycarbonylamino)methyl]phenyl]methyl]carbamate, (**Figure 6G; 9a,** and **Figure 6H**). In contrast, when the same foam was incubated with ROL and ethanol, we found no aromatic dicarbamates but aliphatic tricarbamates resulting from the ethanolysis of the urethane bonds formed with the aliphatic triamine (**Figure 6G; 10b,** and **Figure 6I)**. Moreover, the ethyl-monocarbamate was detected (**Figure 6G: 11b** and **Figure S37**), suggesting the hydrolysis of carbamates upon the transcarbamoylation reaction (**Figure 6G**), following a similar sequential mechanism as the one proposed for TDI-PUR foams. When these NI-PUR foams were incubated with TLL in water, the foam deterioration was very limited according to SEM images, and diamines were not detected by UPLC-MS, in agreement with what we observed with the TDI-PUR foams (**Figure S20**). Since lipase-driven alcoholysis degrades NI-PUR foams more extensively than TDI-PUR foams via a similar mechanism, we propose that the higher hydrophilicity of NI-PUR foams promotes deeper lipase diffusion, enabling more thorough depolymerization. In contrast, in the more hydrophobic TDI-PUR foams, lipase activity remains largely confined to the surface, explaining their lower degree of deterioration. Therefore, TLL and ROL exhibit a broad substrate scope, as they are capable of depolymerizing PUR foams of varying compositions, albeit to different extents.

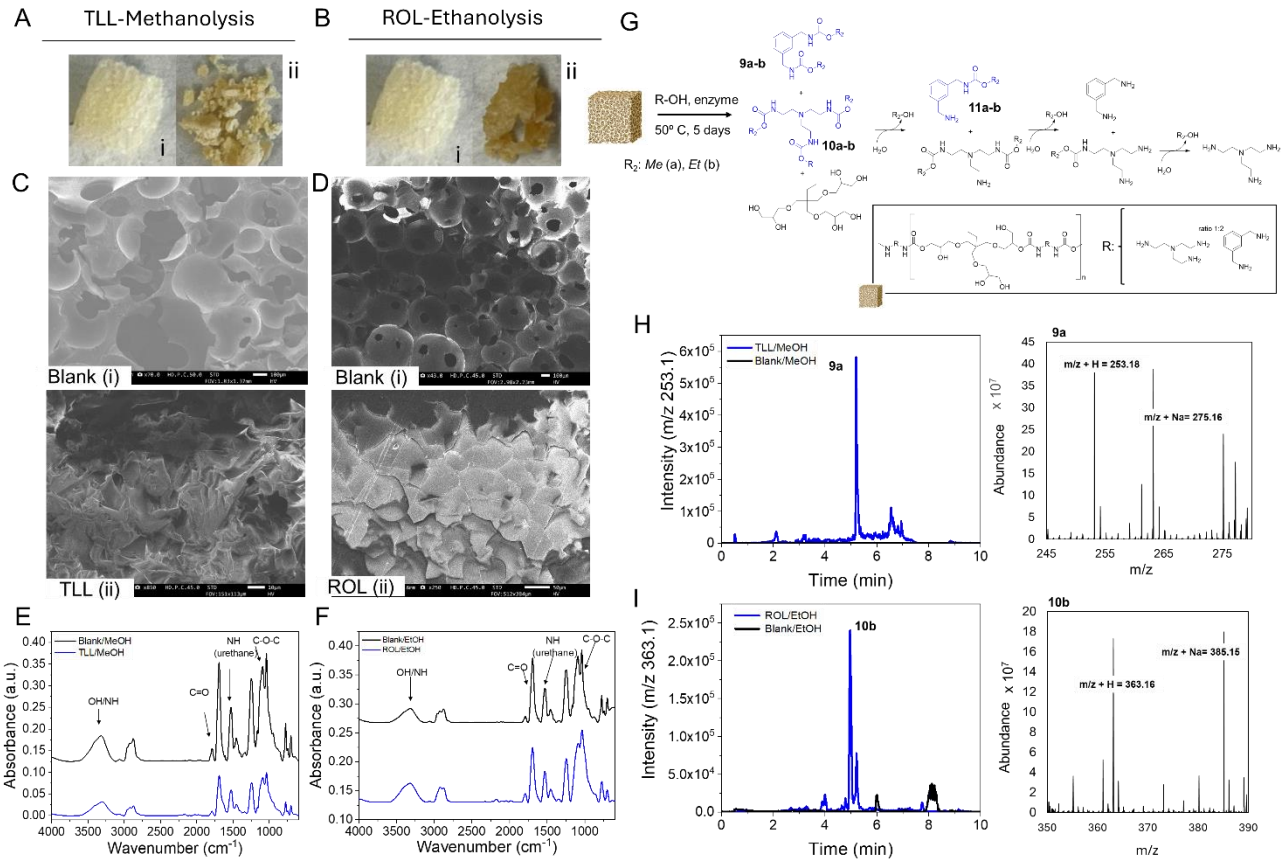

Figure 6: Alcoholysis reactions of NI-PUR foam catalyzed by TLL (**A, C, D,** and **H**) and ROL (**B, E, F,** and **I**) in methanol and ethanol, respectively. Optical (**A** and **B**) and SEM images (**C** and **D**) of foams after 5 days incubation at 50 ºC, in the corresponding alcohol (**A** and **C** for methanol, **B** and **D** for ethanol). Non-treated foam (i) and enzyme-treated foam (ii). FTIR spectra of the resulting foams after methanolysis (**E**) and ethanolysis (**F**) conditions in the presence (blue) and in the absence (black) of the corresponding enzyme. (**G**) Hypothetical reaction scheme if hydrolysis occurs sequentially to alcoholysis, with detected products in blue. UPLC-MS traces (left) and MS spectra (right) of reaction crudes extracted with organic solvents upon methanolysis (**H**) and ethanolysis (**I**). Blue and black traces represent reaction with and without the corresponding lipase, respectively.

When these NI-PUR foams were incubated with TLL in water, the foam deterioration was very limited according to SEM images, and diamines were not detected by UPLC-MS, in agreement with what we observed with the TDI-PUR foams (**Figure S20**). Since lipase-driven alcoholysis degrades NI-PUR foams more extensively than TDI-PUR foams via a similar mechanism, we propose that the higher hydrophilicity of NI-PUR foams promotes deeper lipase diffusion, enabling more thorough depolymerization. In contrast, in the more hydrophobic TDI-PUR foams, lipase activity remains largely confined to the surface, explaining their lower degree of deterioration. Therefore, TLL and ROL exhibit a broad substrate scope, as they are capable of depolymerizing PUR foams of varying compositions, albeit to different extents.

CONCLUSION

In this work, we demonstrate the depolymerization of polyether PUR thermosets formulated as foams through an unconventional enzyme mechanism by exploiting the rare transcarbamoylation reactivity of lipases. After a small enzyme screening, we found two lipases from different microbial sources as specialists for the alcoholysis reaction of PUR

foams. Upon characterizing the treated foams and reaction products, we conclude that both enzymes can erode these foams, changing their physicochemical properties through breaking down the urethane bonds that form their hard segments. Consequently, di and mono-alkylcarbamates are released to the reaction media. Additionally, we isolate the polyether polyols released during the liase-driven methanolysis, which are then used in the fabrication of recycled foams, yielding materials with chemical and structural properties similar to the virgin ones. Here, we demonstrated for the first time an enzymatically driven closed-loop for polyols in TDI-PUR thermoset manufacturing. Still more efforts are needed to isolate methyl dicarbamates with sufficient purity to close a full recycling loop integrating both aromatics and polyols in the manufacturing of recycled foams.
This depolymerization approach has been expanded to other thermoset foams fabricated with the more sustainable non-isocyanate polyurethanes. Despite this unprecedented use of lipase in polymer depolymerization, the yield of released monomers is still limited and needs to be maximized through enzyme and reaction media engineering. Nonetheless, this work illustrates the potential of biocatalysis to move beyond PET in plastic recycling, envisioning the feasibility of enzyme depolymerization of polyether PURs, which has been elusive until now.

Acknowledgments

This work was supported by the Spanish Ministerio de Ciencia, Innovación y Universidades and State Research Agency (AEI) (TED2021-129852B-C21; RT-134755-T; FJC2021-047577-I; FJC2021-004636-C), the European Union's Horizon Europe Research and Innovation Programme under Grant Agreement No. 101099528 (BMREX) and No. 101154935, the Generalitat Valenciana (PROMETEO with ref. CIPROM/2021/079) and Universitat Jaume I (ref. UJI-B-2022-12). The authors wish to thank the staff of the Servei d'Informàtica of the Universitat Jaume I, as well as the local computational resources funded by Generalitat Valenciana - European Regional Development Fund (REF: IDIFEDER/2021/02). We also want to acknowledge to Basque Government for the BIKAINTEK funding (019-B1-2023).

Author contributions

F.L-G, H.S, and V.M conceived the project. R.M and A.R performed the depolymerization studies, D.G-H and M.A-R performed the enzyme characterization studies. I.O and G.P perform all the polymer chemistry studies. R. F-M performed the ATR-FTIR analysis. J.S performed UPLC-MS analysis. K.S performed all computational studies. F.L-G, R.M and D.G-H wrote the first draft of this article. All authors discussed the results and participated in the revision of the paper. V.M, H.S and F.L-G secured the funding.

Competing interests

All authors declare no competing interests.

Data and materials availability

Materials and methods, experimental procedures, phylogenetic analysis, primary sequences of enzymes utilized in this study, analytical data (^{1}H-NMR, MS, UPLC-MS, TGA,

DSC) and computational details to support all the results presented in the manuscript are available in supplementary materials.

References

1. R. Geyer, J. R. Jambeck, K. L. Law, Production, use, and fate of all plastics ever made. *Sci Adv* **3**, e1700782 (2017).
2. S. Wu, S. Ma, Q. Zhang, C. Yang, A comprehensive review of polyurethane: Properties, applications and future perspectives. *Polymer* **327**, 128361 (2025).
3. A. Gomez-Lopez, F. Elizalde, I. Calvo, H. Sardon, Trends in non-isocyanate polyurethane (NIPU) development. *Chem Commun* **57**, 12254-12265 (2021).
4. V. R. Dhara, R. and Dhara, The Union Carbide disaster in Bhopal: a review of health effects. *Arch Environ Health* **57**, 391-404 (2002).
5. N. Fanjul-Mosteirín, L. P. Fonseca, A. P. Dove, H. Sardon, Bio-based non-isocyanate poly(hydroxy urethane)s (PHU) derived from vanillin and CO2. *Mater Adv* **4**, 2437-2448 (2023).
6. A. Hernández *et al.*, Internal catalysis on the opposite side of the fence in non-isocyanate polyurethane covalent adaptable networks. *Eur Polym J* **168**, 111100 (2022).
7. R. Kaur, P. Singh, S. Tanwar, G. Varshney, S. Yadav, Assessment of bio-based polyurethanes: Perspective on applications and bio-degradation. *Macromol* **2**, 284-314 (2022).
8. A. M. Prasad *et al.*, Lab safety alert: a real case of isocyanate exposure. *Polym Chem*, (2025).
9. B. Bizet, É. Grau, H. Cramail, J. M. Asua, Water-based non-isocyanate polyurethane-ureas (NIPUUs). *Polym Chem* **11**, 3786-3799 (2020).
10. M. S. Kathalewar, P. B. Joshi, A. S. Sabnis, V. C. Malshe, Non-isocyanate polyurethanes: from chemistry to applications. *RSC Adv* **3**, 4110-4129 (2013).
11. G. Rokicki, P. G. Parzuchowski, M. Mazurek, Non-isocyanate polyurethanes: synthesis, properties, and applications. *Polym Adv Technol* **26**, 707-761 (2015).
12. H. Sardon *et al.*, Synthesis of polyurethanes using organocatalysis: A perspective. *Macromolecules* **48**, 3153-3165 (2015).
13. Z. Shen *et al.*, A comparison of non-isocyanate and HDI-based poly(ether urethane): Structure and properties. *Polymer* **175**, 186-194 (2019).
14. G. Rossignolo, G. Malucelli, A. Lorenzetti, Recycling of polyurethanes: where we are and where we are going. *Green Chem* **26**, 1132-1152 (2024).
15. R. Heiran *et al.*, Glycolysis: an efficient route for recycling of end of life polyurethane foams. *J Polym Res* **28**, 22 (2021).
16. M. B. Johansen *et al.*, Closed-loop recycling of polyols from thermoset polyurethanes by tert-amyl alcohol-mediated depolymerization of flexible foams. *ACS Sustainable Chem Eng* **11**, 10737-10745 (2023).
17. Y. Deng *et al.*, Reviewing the thermo-chemical recycling of waste polyurethane foam. *J Environ Manage* **278**, 111527 (2021).
18. H.-W. Engels *et al.*, Polyurethanes: Versatile materials and sustainable problem solvers for today's challenges. *Angew Chem Int Ed* **52**, 9422-9441 (2013).
19. A. Kemona, M. Piotrowska, Polyurethane recycling and disposal: Methods and prospects. *Polymers* **12**, 1752 (2020).
20. L. Zhao, V. Semetey, Recycling polyurethanes through transcarbamoylation. *ACS Omega* **6**, 4175-4183 (2021).
21. X. Lopez-Lorenzo, G. Ranjani, P.-O. Syrén, Conformational selection in enzyme-catalyzed depolymerization of bio-based polyesters. *ChemBioChem* **26**, e202400456 (2025).
22. V. Tournier *et al.*, An engineered PET depolymerase to break down and recycle plastic bottles. *Nature* **580**, 216-219 (2020).

23. B. Zhu, Q. Ye, Y. Seo, N. Wei, Enzymatic degradation of polyethylene terephthalate plastics by bacterial curli display PETase. *Environ Sci Technol Lett* **9**, 650-657 (2022).
24. A. Papadopoulou, K. Hecht, R. Buller, Enzymatic PET degradation. *CHIMIA* **73**, 743 (2019).
25. V. Tournier *et al.*, Enzymes' power for plastics degradation. *Chem Rev* **123**, 5612-5701 (2023).
26. N. Mohanan, Z. Montazer, P. K. Sharma, D. B. Levin, Microbial and enzymatic degradation of synthetic plastics. *Front Microbiol* **Volume 11 - 2020**, (2020).
27. J. Benninga, J. Jager, R. Folkersma, V. S. D. Voet, K. Loos, in *Sustainable Green Chemistry in Polymer Research. Volume 1. Biocatalysis and Biobased Materials*. (American Chemical Society, 2023), vol. 1450, chap. 5, pp. 71-87.
28. G. T. Howard, Biodegradation of polyurethane: A review. *Int Biodeterior Biodegrad* **49**, 245-252 (2002).
29. S. P. Katnic, F. M. de Souza, R. K. Gupta, Recent progress in enzymatic degradation and recycling of polyurethanes. *Biochem Eng J* **208**, 109363 (2024).
30. A. Magnin, L. Entzmann, E. Pollet, L. Avérous, Breakthrough in polyurethane bio-recycling: An efficient laccase-mediated system for the degradation of different types of polyurethanes. *Waste Manage* **132**, 23-30 (2021).
31. A. Magnin *et al.*, Enzymatic recycling of thermoplastic polyurethanes: Synergistic effect of an esterase and an amidase and recovery of building blocks. *Waste Manage* **85**, 141-150 (2019).
32. S. Sahu, A. Kaur, M. Khatri, G. Singh, S. K. Arya, A review on cutinases enzyme in degradation of microplastics. *J Environ Manage* **347**, 119193 (2023).
33. R. Salas *et al.*, Biocatalytic hydrolysis of di-urethane model compounds in ionic liquid reaction media. *Catal Today* **430**, 114516 (2024).
34. Y. Branson *et al.*, Urethanases for the enzymatic hydrolysis of low molecular weight carbamates and the recycling of polyurethanes. *Angew Chem Int Ed* **62**, e202216220 (2023).
35. Z. Li *et al.*, Structure-guided engineering of a versatile urethanase improves its polyurethane depolymerization activity. *Adv Sci* **12**, 2416019 (2025).
36. T. Bayer *et al.*, Structural elucidation of a metagenomic urethanase and its engineering towards enhanced hydrolysis profiles. *Angew Chem Int Ed* **63**, e202404492 (2024).
37. E. Luna *et al.*, Towards a better understanding of the cosolvent effect on the low-temperature glycolysis of Polyethylene Terephthalate (PET). *Chem Eng J* **482**, 148861 (2024).
38. G. Carrea, S. Riva, Properties and synthetic applications of enzymes in organic solvents. *Angew Chem Int Ed* **39**, 2226-2254 (2000).
39. A. Zaks, A. M. Klibanov, Enzymatic catalysis in organic media at 100°C. *Science* **224**, 1249-1251 (1984).
40. A. Zaks, A. M. Klibanov, Enzyme-catalyzed processes in organic solvents. *PNAS* **82**, 3192-3196 (1985).
41. A. Zaks, A. M. Klibanov, Substrate specificity of enzymes in organic solvents vs. water is reversed. *J Am Chem Soc* **108**, 2767-2768 (1986).
42. A. Zaks, A. M. Klibanov, Enzymatic catalysis in nonaqueous solvents. *J Biol Chem* **263**, 3194-3201 (1988).
43. M. M. C. H. van Schie, J.-D. Spöring, M. Bocola, P. Domínguez de María, D. Rother, Applied biocatalysis beyond just buffers – from aqueous to unconventional media. Options and guidelines. *Green Chem* **23**, 3191-3206 (2021).
44. S. M. Meza Huaman, J. H. Nicholson, A. P. S. Brogan, A general route to retooling hydrolytic enzymes toward plastic degradation. *Cell Rep Phys Sci* **5**, 101783 (2024).
45. S. Kobayashi, H. Uyama, T. Takamoto, Lipase-catalyzed degradation of polyesters in organic solvents. A new methodology of polymer recycling using enzyme as catalyst. *Biomacromolecules* **1**, 3-5 (2000).
46. A. Bajaj, P. Lohan, P. N. Jha, R. Mehrotra, Biodiesel production through lipase catalyzed transesterification: An overview. *J Mol Catal B: Enzym* **62**, 9-14 (2010).
47. K. Nie, F. Xie, F. Wang, T. Tan, Lipase catalyzed methanolysis to produce biodiesel: Optimization of the biodiesel production. *J Mol Catal B: Enzym* **43**, 142-147 (2006).

48. S. Xia, J. Lin, S. Sayanjali, C. Shen, L.-Z. Cheong, Lipase-catalyzed production of biodiesel: a critical review on feedstock, enzyme carrier and process factors. *Biofuels Bioprod Biorefin* **18**, 291-309 (2024).
49. A. Magnin, E. Pollet, L. Avérous, in *Methods in Enzymology,* G. Weber, U. T. Bornscheuer, R. Wei, Eds. (Academic Press, 2021), vol. 648, pp. 317-336.
50. S. Bendicho, M. C. Trigueros, T. Hernández, O. Martín, Validation and comparison of analytical methods based on the release of *p*-nitrophenol to determine lipase activity in milk. *J Dairy Sci* **84**, 1590-1596 (2001).
51. A. M. Farnet *et al.*, A modified method based on *p*-nitrophenol assay to quantify hydrolysis activities of lipases in litters. *Soil Biol Biochem* **42**, 386-389 (2010).
52. G. Pencreac'h, J. C. Baratti, Hydrolysis of p-nitrophenyl palmitate in n-heptane by the *Pseudomonas cepacia* lipase: A simple test for the determination of lipase activity in organic media. *Enzyme Microb Technol* **18**, 417-422 (1996).
53. N. Kébir, M. Benoit, C. Legrand, F. Burel, Non-isocyanate thermoplastic polyureas (NIPUreas) through a methyl carbamate metathesis polymerization. *Eur Polym J* **96**, 87-96 (2017).
54. E. Abreu Silveira *et al.*, Biocatalyst engineering of *Thermomyces Lanuginosus* lipase adsorbed on hydrophobic supports: Modulation of enzyme properties for ethanolysis of oil in solvent-free systems. *J Biotechnol* **289**, 126-134 (2019).
55. A. Millqvist, P. Adlercreutz, B. Mattiasson, Lipase-catalyzed alcoholysis of triglycerides for the preparation of 2-monoglycerides. *Enzyme Microb Technol* **16**, 1042-1047 (1994).
56. M. M. Soumanou, U. T. Bornscheuer, Lipase-catalyzed alcoholysis of vegetable oils. *Eur J Lipid Sci Technol* **105**, 656-660 (2003).
57. Y.-d. Wang *et al.*, Immobilized recombinant *Rhizopus oryzae* lipase for the production of biodiesel in solvent free system. *J Mol Catal B: Enzym* **67**, 45-51 (2010).
58. K. Griebenow, A. M. Klibanov, On protein denaturation in aqueous−organic mixtures but not in pure organic solvents. *J Am Chem Soc* **118**, 11695-11700 (1996).
59. M. Salaheldeen *et al.*, Current state and perspectives on transesterification of triglycerides for biodiesel production. *Catalysts* **11**, 1121 (2021).
60. A. Fernández, O. Sinanoğlu, Denaturation of proteins in methanol/water mixtures. *Biophys Chem* **21**, 163-166 (1985).
61. M. Pazhang, N. Mardi, F. Mehrnejad, N. Chaparzadeh, The combinatorial effects of osmolytes and alcohols on the stability of pyrazinamidase: Methanol affects the enzyme stability through hydrophobic interactions and hydrogen bonds. *Int J Biol Macromol* **108**, 1339-1347 (2018).
62. R. Fernandez-Lafuente, Lipase from *Thermomyces lanuginosus*: Uses and prospects as an industrial biocatalyst. *J Mol Catal B: Enzym* **62**, 197-212 (2010).
63. A. M. Brzozowski *et al.*, Chemical Reviews. *Biochemistry* **39**, 15071-15082 (2000).
64. M. E. Viana, A. Riul, G. M. Carvalho, A. F. Rubira, E. C. Muniz, Chemical recycling of PET by catalyzed glycolysis: Kinetics of the heterogeneous reaction. *Chem Eng J* **173**, 210-219 (2011).
65. S. Oprea, Dependence of fungal biodegradation of PEG/castor oil-based polyurethane elastomers on the hard-segment structure. *Polym Degrad Stab* **95**, 2396-2404 (2010).
66. M. Spontón *et al.*, Biodegradation study by *Pseudomonas sp*. of flexible polyurethane foams derived from castor oil. *Int Biodeterior Biodegrad* **85**, 85-94 (2013).
67. A. Magnin, E. Pollet, V. Phalip, L. Avérous, Evaluation of biological degradation of polyurethanes. *Biotechnol Adv* **39**, 107457 (2020).
68. T. B. Phan, H. Mayr, Comparison of the nucleophilicities of alcohols and alkoxides. *Can J Chem* **83**, 1554-1560 (2005).
69. I. Olazabal *et al.*, Upgrading polyurethanes into functional ureas through the asymmetric chemical deconstruction of carbamates. *ACS Sustainable Chem Eng* **11**, 332-342 (2023).
70. S. M. Arnold *et al.*, Risk assessment for consumer exposure to toluene diisocyanate (TDI) derived from polyurethane flexible foam. *Regul Toxicol Pharm* **64**, 504-515 (2012).